Development of red-emissive porphyrin graphene quantum dots (PGQDs) for biological cell-labeling applications

Sarah Reagen[1], Yingfen Wu[1], Rahul Shahni[1], Wen Sun[1], Jin Zhang[2], Qianli R. Chu[1], Xiaodong Hou[2], Colin Combs[3], and Julia Xiaojun Zhao[1*]

[1]Department of Chemistry, University of North Dakota, Grand Forks, ND 58202, USA

[2]Institute for Energy Studies, University of North Dakota, Grand Forks, ND 58202, USA

[3]Department of Biomedical Sciences, University of North Dakota, Grand Forks, North Dakota 58202, USA

Abstract

Red and near infrared emission is a highly desirable feature for fluorescent nanoparticles in biological applications mainly due to longer wavelengths more easily being able to deeply penetrate tissues, organs, skin, and other organic components while less autofluorescence interference would be produced. Additionally, graphene quantum dots (GQDs) that contain unique optical and electrical features have been targeted for their use in cell labeling applications as well as environmental analysis. Their most desirable features come in the form of low toxicity and biocompatibility; however, GQDs are frequently reported to have blue or green emission light and not the more advantageous red/NIR emission light. Furthermore, porphyrins are a subgroup of heterocyclic macrocycle organic compounds that are also naturally occurring pigments in nature that already contain the desired red-emission fluorescence. Therefore, porphyrins have been used previously to synthesize nanomaterials and for nanoparticle doping in order to incorporate the red/NIR emission light property into particles that otherwise do not contain the desired emission light. Meso-tetra(4-carboxyphenyl)porphine (TCPP) is one type of porphyrin with a large conjugated π-electron system and four carboxyl groups on its exterior benzene rings. These two key characteristics of TCPP makes it ideal for incorporation into GQDs as it would design and synthesize red-emissive material as well as give rise to excellent water solubility. In this work, TCPP is used in tangent with *cis*-cyclobutane-1,2-dicarboxylic acid (CBDA-2), a biomass derived organic molecule, to synthesize "green" porphyrin-based graphene quantum dots (PGQDs) with red-emission. The obtained PGQDs were characterized by various analytical methods Utilizing TEM, HRTEM, and DLS the size distribution of the particles was determined to be 7.9 ± 4.1, well within the quantum dot range of 2-10 nm. FT-IR, XPS, and XRD depicted carbon, nitrogen, and oxygen as the main elemental components with carbon being in the form of graphene and the main porphyrin ring of TCPP remaining present in the final PGQDs product. Lastly, absorption and fluorescence spectroscopy determined the excitation wavelength at 420 nm and the emission at 650 nm which was successfully utilized in the imaging of HeLa cells using confocal microscopy.

Keywords: nanoparticles, porphyrin, graphene, quantum dots, in vitro, cell imaging

1. Introduction

Graphene quantum dots (GQDs) are a subset of semiconductor carbon-based nanoparticles that are defined by their size limitation, being 2-10 nm in diameter.[1,2] GQDs contain unique optical and electrical features that are attributed to the sp^2-hybridized carbon atoms within the lattice of the GQDs which allows them to have a π-conjugated system.[3] This property allows GQDs to be utilized primarily in biological, biomedical, and biosensing fields of study. More specifically, their unique quenching properties enable them to be used for environmental analysis as well as biological, typically in the form of trace molecules, metal ions, cation, and anion detection.[4-7] Additionally, their carbon-based makeup of graphene gives GQDs a low cytotoxicity, further enhancing their use in biological matrices and cell imaging applications. However, GQDs have been reported to typically have blue or green emission light[7-9], which is not optimal for cellular imaging, as shorter wavelength emission light cannot as effectively penetrate tissues, organs, skin, etc. in a biological setting due to light scattering.[10] Red or near infrared (NIR) emission light is a more suitable option for biological imaging, especially for *in vitro* and *in vivo* confocal microscopy.[10,11] However, as previously stated, GQDs and carbon-based nanomaterials are scarcely reported to be synthesized to have a red or NIR emission light.[12] Therefore, researchers have investigated alternative synthesis methods to address this issue and give new GQDs a longer wavelength emission. One such method involves doping GQDs with other elements (nitrogen[13], metals[14,15], etc.) or other nanoparticles[16].

Subsequently, a subgroup of organic molecules that have recently become of interest are porphyrins which, much like GQDs, have unique optical, electrical, and biological properties. Porphyrins are a class of heterocyclic macrocycle organic compounds that are commonly found in nature such as in redox active enzymes like hemoglobin and cytochromes as well as in plant photosynthetic apparatuses.[17] In recent history, porphyrin-based materials have primarily been used for chemical and ion sensing[18], photocatalysis[19], light harvesting[20], and photothermal therapy[21,22]. Porphyrins naturally contain red-emissive fluorescence making them useful for biological imaging applications, however, like other fluorescent dyes, porphyrins lack photostability for prolonged imaging analysis as well as contain self-quenching problems.[23]

To overcome the poor photostability of porphyrins, in combination with an additional photostable carbon molecule may be useful. *Cis*-3,4-di(furan-2-yl)cyclobutane-1,2-dicarboxylic acid (CBDA-2) was used previously and successfully synthesized GQDs with exceptional photostability and cytotoxicity, however, it contained the common

emission peak of 440 nm and therefore did not contain the desired red-emission.[24] Considering the above mentioned properties of porphyrins and CBDA-2, the goal of this research is to develop porphyrin-based graphene quantum dots (PGQDs) for enhanced red-emission nanomaterial for bioimaging and metal ion detection applications. Meso-tetra(4-carboxyphenyl)porphine (TCPP) is one type of porphyrin with a large conjugated π-electron system and four carboxyl groups on its exterior benzene rings. Given that TCPP has successfully been used previously to nanomaterial synthesis[23] and biological imaging[25] and sensing[26] applications, here, TCPP has also been selected for the porphyrin of choice, while the main carbon contribution will be supplied from biomass-derived CBDA-2 to form PGQDs. Additionally, utilizing CBDA-2, a biomass-derived molecule due to it being derived from furfural[27], makes this process a synthetically green reaction and the resulting environmentally friendly PGQDs.

2. Experimental

2.1. Materials

3-(Cyclohexylamino)-1-propanesulfonic acid (CAPS buffer, ≥99%), 2-(cyclohexylamino)ethanesulfonic acid (CHES buffer, ≥99%), 2-[4-(2-hydroxyethyl)piperazin-1-yl]ethanesulfonic acid (HEPES buffer, 99.5%), citric acid (≥99.5%), maleic acid (≥99%), meso-tetra(4-carboxyphenyl)porphine (TCPP). $FeCl_3$, $Pb(Ac)_2 \cdot 3H_2O$, and $CuSO_4$ were purchased from Sigma-Aldrich (St. Louis, MO, USA). $HgCl_2$ was purchased from ACROS Organics (Fair Lawn, NJ, USA). Micro cover glass and $FeSO_4 \cdot 7H_2O$ was purchased from Sargent-Welch VWR Scientific (Buffalo Grove, IL, USA). Fluorescein dye along with ammonium hydroxide (99%) and 96-well plate were purchased from Fisher Scientific (Hampton, NG, USA). CytoTox 96 Non-Radioactive Cytotoxicity Assay kit (showed as LDH assay in following sections) was purchased from Promega (Madison, WI, USA). Deionized (DI) water was produced by a Millipore water purification system (18.3 Ω · cm). HeLa cell line was purchased from ATCC (Manassas, VA, USA). Cell culture media, penicillin-streptomycin and trypsin were purchased from Gibco (Waltham, MA, USA). 4% paraformaldehyde (PFA) was purchased from Electron Microscopy Sciences (Hatfield, PA, USA). Fetal bovine serum (FBS) was purchased from Peak Serum, Inc (Wellington, CO, USA). Fluoromount-G mounting media was purchased from Southern Biotech (Birmingham, AL, USA). 96-well plate was purchased from Thermo Fisher Scientific (Waltham, MA, USA). Cell culture plates were purchased from Greiner Bio One (Kremsmunster, Austrian). Lab-Tek II Chamber Slide system was purchased from Nalge Nunc International Corp (Naperville, IL, USA).

2.2. Sample solution preparation

The buffer solutions of CAPS, CHES, HEPES, citric acid, and maleic acid were prepared in concentrations of 20 mM and the pHs of 1.0, 3.0, 5.0, 7.0, 9.0, and 11.0 were adjusted by the addition of NaOH or HCl. For experiments of investigating photostability, dynamic light scattering, and zeta potential measurements, samples were sonicated for 10 - 30 min before analysis. For the detection of metal ions, 1.0 mM solutions of $CuSO_4$, $FeCl_3$, $FeSO_4$, $Pb(Ac)_2$, and $HgCl_2$ were prepared in DI-water for further dilutions as needed.

2.3. Instrumentation for the characterization of porphyrin-based GQDs

A Perkin Elmer Lambda 1050 UV-250 UV/Vis/NIR spectrophotometer was used for the UV-Vis absorption measurements of the PGQDs. The fluorescence spectra and photostability measurements were acquired by a Shimadzu RF-6000 spectrophotometer. A Marlvern model of Nano-ZS Zetasizer was used to measure size distribution of the PGQDs as well as the zeta potential at various pHs. A Thermo Fisher Scientific Nicolet iS5 Fourier transform infrared spectrometer (FT-IR) was utilized to obtain the IR spectra of PGQDs, TCPP, CBDA-2 and the GQDs. A Hitachi 7500 Transmission Electron Microscope (TEM) and a JEOL JEM-F200 High-resolution Transmission Electron Microscope (HRTEM) were used for particle imaging. Powder X-ray diffraction (XRD) measurement was conducted on a Rigaku SmartLab X-ray diffractometer at a scan rate of 4 °/min with Cu Kα irradiation ($\lambda = 0.15418$) at an accelerating voltage of 40 kV and a tube current of 44 mA. The fine powder sample was loaded on a zero-background silicon wafer sample holder. An Olympus FV1000 MPE Basic Multiphoton Microscope was used for *in vitro* confocal imaging. HeLa cells were cultured over night with gradient concentrations of the PGQDs for *in vitro* imaging and cytotoxicity analysis. A ELX800 plate reader was used for the cell viability experiments using the protocol of CytoTox 96 Non-Radioactive Cytotoxicity Assay kit.

2.4. Synthesis of PGQDs

16.0 mg of CBDA-2 and 12.5 mg of TCPP were dissolved in 15.0 mL of DI-water and 100 µL of ethylenediamine before sonication for 30 min. The resulting solution was then autoclaved for 12 h at 200 °C. After those 12 h the solution was removed and allowed to cool to room temperature before filtration using a 0.22 µm syringe filter and then dialyzed for 3 days using a 500-1000 Da membrane against DI-water. When exposed to UV light, the PGQDs solution visibly showed red-emission light compared to GQDs blue-emission.

2.5. Quantum yield measurement

The quantum yield of the PGQDs (650 nm) peak in HEPES buffer pH 7.0 was calculated against quinine sulfate in 0.1 M H_2SO_4 (Φ_{st} of 0.54) and FITC in 0.1 M NaOH (Φ_{st} of 0.79) as both were used as the standard reference.[28] Calibration curves of fluorescence intensity *vs* absorbance for the PGQDs and standard references were generated and, utilizing Equation 1 below, the quantum yield of PGQDs was calculated to be 46.6% against both standards; where Φ_x is the fluorescence quantum yield of the PGQDs, Φ_{st} is the quantum yield of the standard, $Grad_x$ and $Grad_{st}$ are the gradients of the calibration curve fluorescence intensity *vs* absorbance for the PGQDs and standards, respectively. η_x and η_{st} are the refractive index of the solvents for the PGQDs and standards. This is an exceptional quantum yield for graphene-based quantum dots, and additionally acceptable for PGQDs as well.

$$\Phi_x = \Phi_{st}\left(\frac{Grad_x}{Grad_{st}}\right)\left(\frac{\eta_x^2}{\eta_{st}^2}\right) \quad \text{(Eq. 1)}$$

2.6. Cell toxicity and imaging experiments

The viability of cells exposed to PGQDs was tested with a CytoTox 96® Non-Radioactive Cytotoxicity Assay kit. Briefly, the cells were incubated with PGQDs in a 96-well plate overnight. A gradient concentration of PGQDs (0, 1, 5, 10, 20, 50, 100, and 200 μg/mL) was added into the wells. After 24 h, 50 μL aliquots of media from all groups were transferred to a new 96-well plate and mixed with 50 μL of the CytoTox 96 Reagent solution. After a 30 min incubation in the dark, 50 μL of the Stop Solution were added to the wells and viability was assessed by reading absorbance at 490 nm.

HeLa cells were plated into an 8-well chamber slide overnight for *in vitro* imaging. 20 mg/mL PGQDs were added into different wells for 3 h while a control was prepared for each sample. Then the slide was washed with PBS and the cells were fixed with 4% paraformaldehyde (PFA). The chamber wells were removed, and the slide was coverslipped for imaging

3. Results and Discussions

3.1. Design of the PGQDs

A key component of this synthesis is using a biomass-derived molecule, making the product synthetically "green" and environmentally friendly. CBDA-2 was successfully derived from hemicellulose taken from agriculture corn waste products through a serious of chemical reactions including Knoevenagel condensation and blacklight

radiation.[27] There are several means of which to incorporate the red-emission into GQDs as discussed previously. Keeping true to the use of natural material in order to reduce waste and the use of harmful chemicals, porphyrins were examined as an alternative. Given the status of porphyrins being pigments found throughout nature in several different forms, these unique molecules already contain the highly desirable red-emission. However, like other fluorescent dyes and pigments, porphyrins suffer from poor photostability and photobleaching. The design of this experiment is to utilize the strengths of both porphyrins and CBDA-2 such that they counter each other's weaknesses. In this work, the porphyrin TCPP was chosen to be incorporated with CBDA-2 due to its successful use in nanoparticle synthesis in other studies[29]. Given that the use of porphyrins to synthesize nanoparticles is limited, and to minimize potential unforeseen issues in the synthesis procedure, it was vital to use a porphyrin that was successfully used previously when used in this work because the two components of CBDA-2 and TCPP have never been used in tandem. The synthesis route was shown in Schematic 1.

To synthesize the PGQDs, 20.0 mg CBDA-2 and 16.0 mg TCPP were dissolved in 20 mL of DI-water. To aid the compounds dissolving, the solution pH needs to be adjusted to a basic pH of 10.0 for CBDA-2. NH_4OH was used for this pH adjustment before autoclaving the sample at 200 °C for 12 h. The resulting solution was allowed to cool to room temperature before it was filtered with a 0.22 µm syringe filter and subjected to dialysis for 3 days against a 500-1000 Da membrane. Although GQDs contain an absorption at approximately 300 nm, the PGQDs showed a strong absorption peak at 420 nm which is consistent with TCPP absorption (416 nm), just slightly shifted. However, despite filtration and dialysis, residual TCPP was still accumulated in the solution as Q-bands were observed in the range of 475 – 655 nm, which are not typically retained after synthesis into forms of nanoparticles (Figure 1).

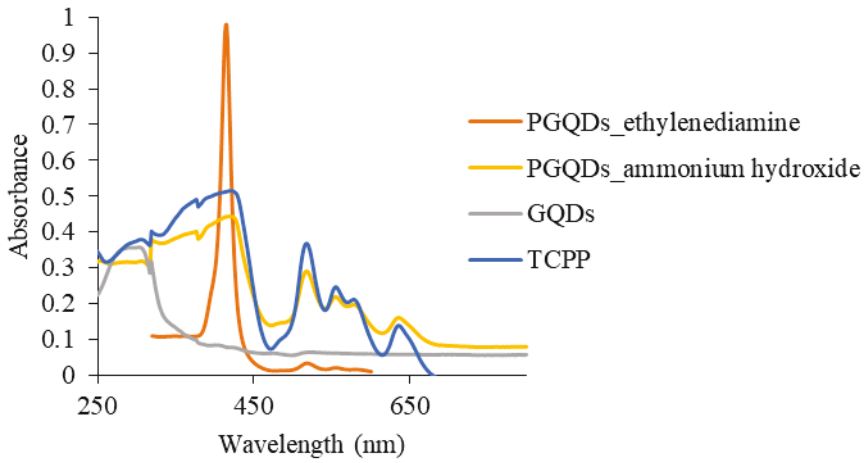

Figure 1: Synthesis of PGQDs utilizing NH_4OH (75 µg/mL) and ethylenediamine (40 µg/mL) compared to GQDs (20 µg/mL) previously synthesized and TCPP (50 µg/mL).

To resolve this issue of residual TCPP and Q-bands, the synthesis was adjusted and instead of using NH_4OH to dissolve CBDA-2 and TCPP, 100 µL ethylenediamine was used due to its greater nucleophilic tendencies toward oxygen functional groups on the formed GQDs.[30] The rest of the reaction synthesis remained the same (Schematic 1) and after dialysis, the PGQDs were dried at 60 °C in an autoclave oven which also helped remove any residual TCPP while still containing the red-emissive particles, as discussed later.

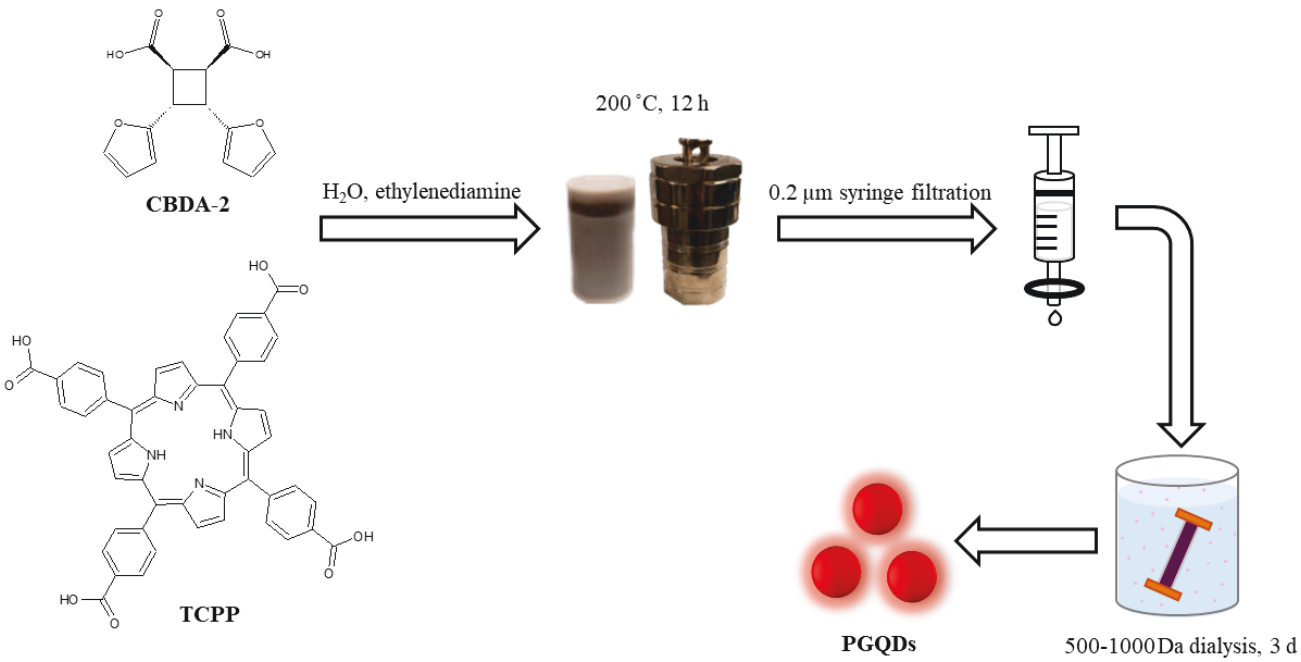

Schematic 1: Combination of CBDA-2 and TCPP to synthesize PGQDs. Experimental conditions: 200 °C for 12 h before 0.2 µm syringe filtration and dialysis for 3 d in 500-1000 Da membrane against DI-water.

3.2. Characterization of PGQDs

3.2.1. Morphology and size of PGQDs

QDs have a strict size definition of 2-10 nm and therefore it is essential to determine the size distribution of the newly synthesized particles to ensure their characterization as QDs. To do this, the morphology of the PGQDs was characterized using both regular TEM and high-resolution TEM (HRTEM). TEM images were first acquired (Figure 2A), which depicted large particles clusters; the largest being 24.7 nm and smaller particles ranging from 2.7-4.7 nm. The smaller particles were more abundant than the larger particles, however, the lower resolution of the TEM images made it difficult to distinguish clusters from large individual particles. Therefore, HRTEM images were also examined in order to better differentiate particles from each other. HRTEM images (Figure 2B) depicted particles with an average diameter of 7.5 nm. Furthermore, the internal graphene lattice was visible in the image. However, additional

complications arose with HRTEM imaging as the carbon-based PGQDs were set against a carbon mesh, resulting in the smaller particles fading into the background and becoming difficult to accurately measure the lattice size. To confirm the graphene lattice, XRD of the PGQDs was analyzed, which will be discussed later.

With the HRTEM carbon-mesh imaging complications, and after seeing some agglomeration of the PGQDs in the TEM images, the particles were analyzed by DLS at various concentrations with various sonication times in order to optimize conditions for minimal agglomeration and more accurate determine particle size distribution. Ultimately, it was found that the sonication time was proportional to the concentration of PGQDs. Lower concentrations required less sonication time. If sonication was prolonged, the PGQDs would agglomerate. Concentrations of 5.0 μg/mL only required 5 min of sonication to limit agglomeration, however, exceeding 10 min of sonication showed a drastic increase in agglomeration. The same was true of higher concentrations, such as 30 μg/mL, which required a minimum sonication time of 30 min, but could not exceed 60 min without showing the same drastic increase in agglomeration. The optimal conditions for PGQDs to limit agglomeration was 5-30 μg/mL with proportional sonication times, not exceeding 60 min for the highest concentration (Figure 2C). The average particle size utilizing DLS was 7.9 ± 4.1 nm which is consistent with the observable particles in both the TEM and HRTEM images.

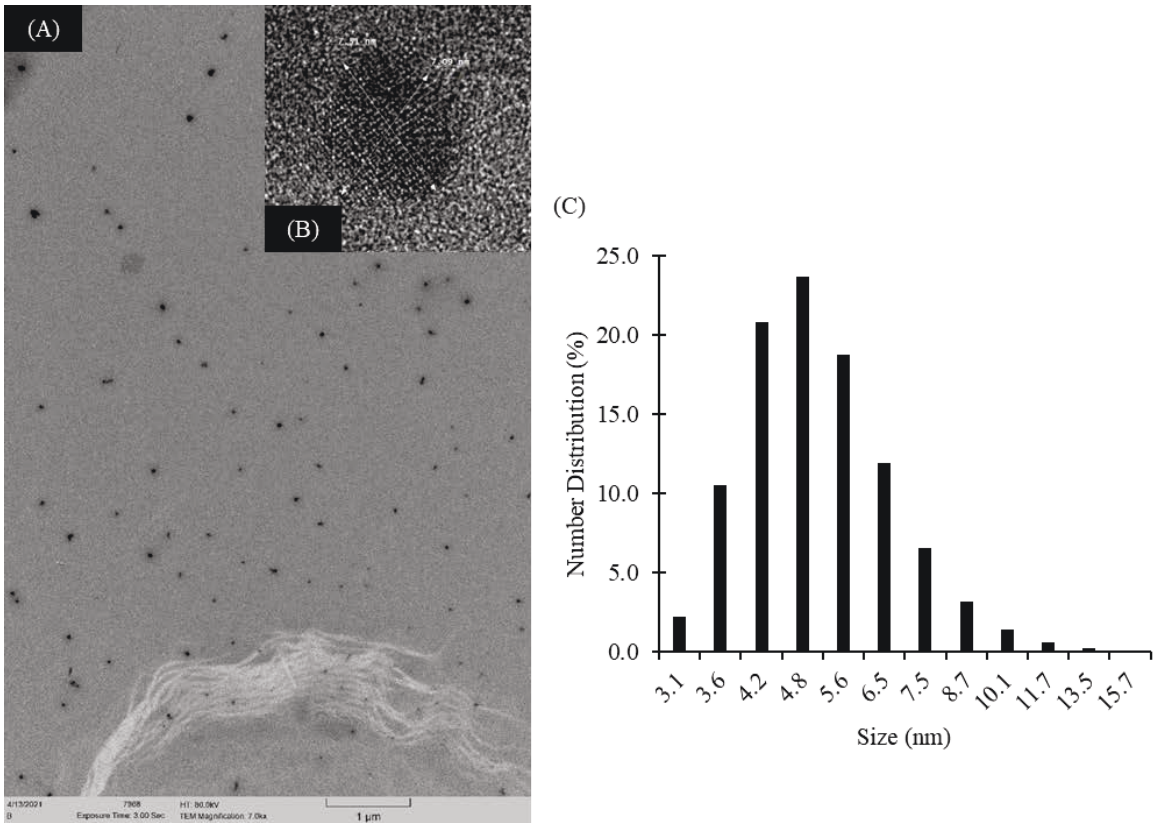

Figure 2: TEM images of 750 µg/mL PGQDs; (A) TEM image of cluster with particles 2.7 – 4.7 nm in size. (B) HRTEM image of single 7.5 nm particle with graphene lattice. (C) DLS analysis of 5 µg/mL PGQDs in DI-water (sonicated for 5-10 min). An average particle size was found to be 7.9 ± 4.1 nm.

3.2.2. Surface functional groups and elemental characterization of PGQDs

With the morphology and size characterization of the PGQDs showing encouraging results, further analysis was required to better understand the composition of the PGQDs. Therefore, the elemental makeup and functional group formation needed to be determined. The initial particle surface characterization was found through zeta potential, an electrical potential found at the slipping plane, of particles in suspension that is used to help predict surface interactions and long-term stability. Zeta potential of particles is also valuable to determine whether the particles could be used in biological applications, as the surface charge of the particles impacts their interaction with the surface of the cell. However, there are many factors that affect zeta potential and one of the more important factors is pH. More basic conditions will result in a buildup of negative charge while acidic conditions will build up a positive charge. Depending on the charge of the particles, switching the charge to positive or negative can result in the particles' surface charge being neutralized, resulting in a zero zeta potential that causes the particles to agglomerate and fall out

of suspension. Due to these particles being targeted for biological applications, it is vital to determine that the PGQDs are stable in neutral pHs and do not agglomerate.

Therefore, the zeta potentail of PGQDs was tested in a pH range of 1.0 - 11.0, and the PGQDs depict an interesting trend. Despite the pH range of 1.0 - 11.0, the PGQDs showed relatively stable zeta potentials throughout compared to regular GQDs[24] with no clear linear trend (Figure 3). This is most likely due to the nitrogen in TCPP that can maintain a positive charge in solution with decreasing pH as traditional GQDs do not contain nitrogen groups for positive charge stability. The most stable zeta potential was observed at pH 11.0 (-35.0 mV), which then decreases in pH 9.0 (-23.6 mV) and 7.0 (-22.2 mV) before slightly increasing in pH 6.5 (-24.8 mV) and pH 5.0 (-27.8 mV). This slight increase in the more neutral-acidic region could be due to equilibrium forming between the negative charge on oxygen groups and the positive charge on nitrogen groups. After pH 5.0, the zeta potential flips positive for pH 3.0 (+22.7 mV) and pH 1.0 (+23.8 mV), however, the potential is still showing mild stability indicating that the particles are not agglomerating due to the nitrogen groups on TCPP withstanding the pH change and increase positive charge in solution. Additionally, between pH 5.0 and 3.0 is the isoelectric point, at approximately pH 3.9, and therefore this is where aggolmeration is most likely to occur and where solution is least stable.

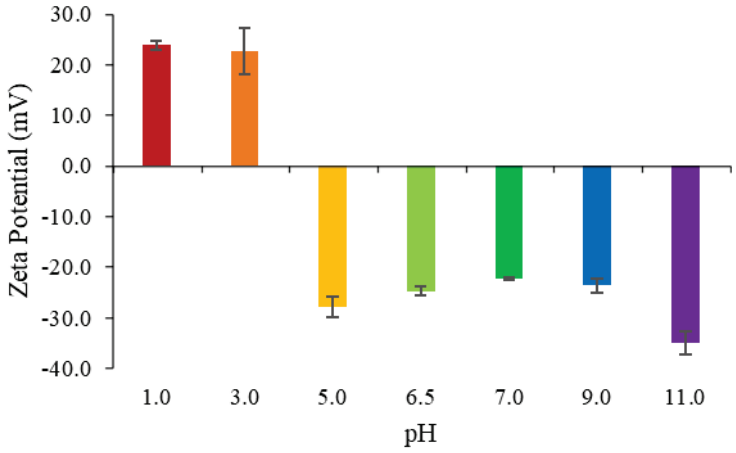

Figure 3: Zeta potential measurements of 38 µg/mL PGQDs in pH 1.0-11.0 buffer solutions after 30 min sonication.

The surface functional groups were characterized using FT-IR. The FT-IR spectra of GQDs, PGQDs, CBDA-2 and TCPP (Figure 4) were analyzed to determine functional groups and any chemical changes that occurred during the synthesis process. For the PGQDs, it was observed that the streching vibration frequency (black dashed line) of

carbonyl attached to porphyrin macrocycles was missing compared to TCPP. Additionally, PGQDs contain C=C (1647 cm^{-1}, green (a)) and C=N (1541 cm^{-1}, blue (b)) double bonds that are broadened, suggesting a chemical change and the formation of QDs. PGQDs also contain the same C=N peak (1378 cm^{-1}, yellow (c) green dashed line) that is also observed in TCPP, suggesting that the porphyrin ring was maintained throughout the synthesis that was contributing to the PGQDs fluorescence characteristics.[31]

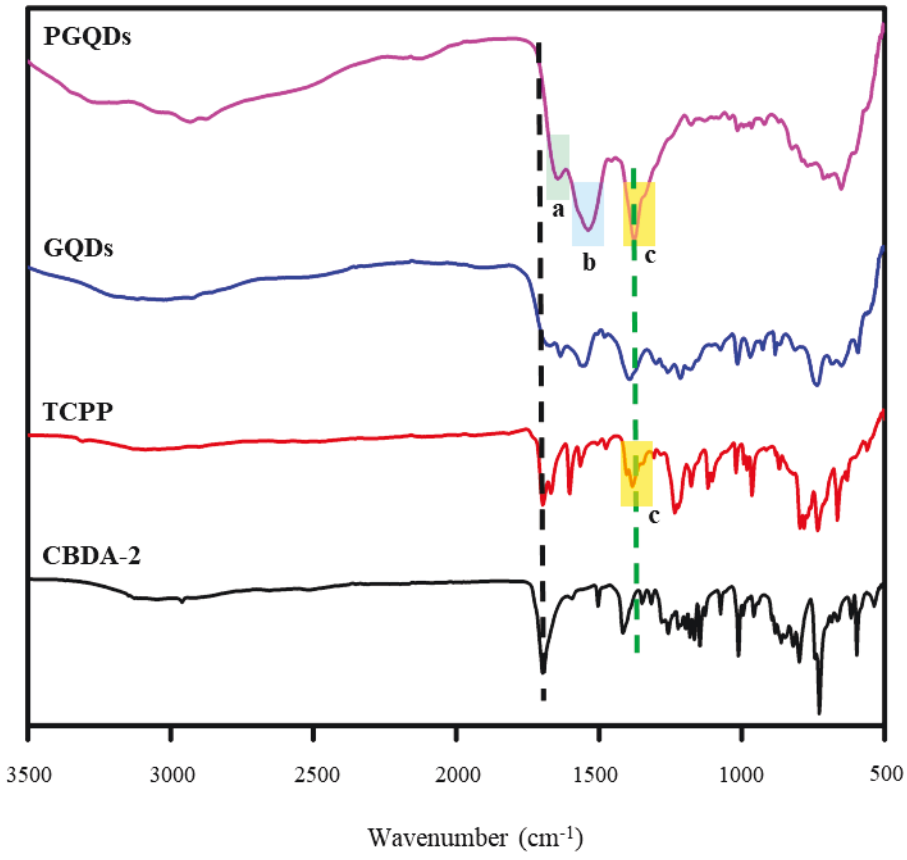

Figure 4: FT-IR spectra of GQDs, PGQDs, TCPP, and CBDA-2, all dried to a solid powder.

The presence of these functional groups was confirmed with the use of XPS, a form of elemental analysis. The XPS spectrum (Figure 5A) shows three distinct element peaks of carbon (285 eV), nitrogen (400 eV), and oxygen (533 eV). This is consistent with the elements observed in both starting compounds and the bonds observed in FT-IR. Both TCPP and CBDA-2 contribute to the oxygen and carbon peaks while only TCPP will contain nitrogen, further confirming the presence of the porphyrin ring being maintained through the synthesis process. This also explains the abundance of carbon and oxygen compared to nitrogen.

Additionally, the graphene lattice is essential in this work as its formation aids in the structural stabilization of the particles compared to carbon quantum dots without the internal lattice due to different hybridization. To confirm the graphene lattice, XRD of the PGQDs was analyzed. A shallow peak at 20° in the XRD spectrum of the PGQDs (Figure 5B) points to carbon in a graphene lattice[32] while no other peaks were observed in the spectrum.

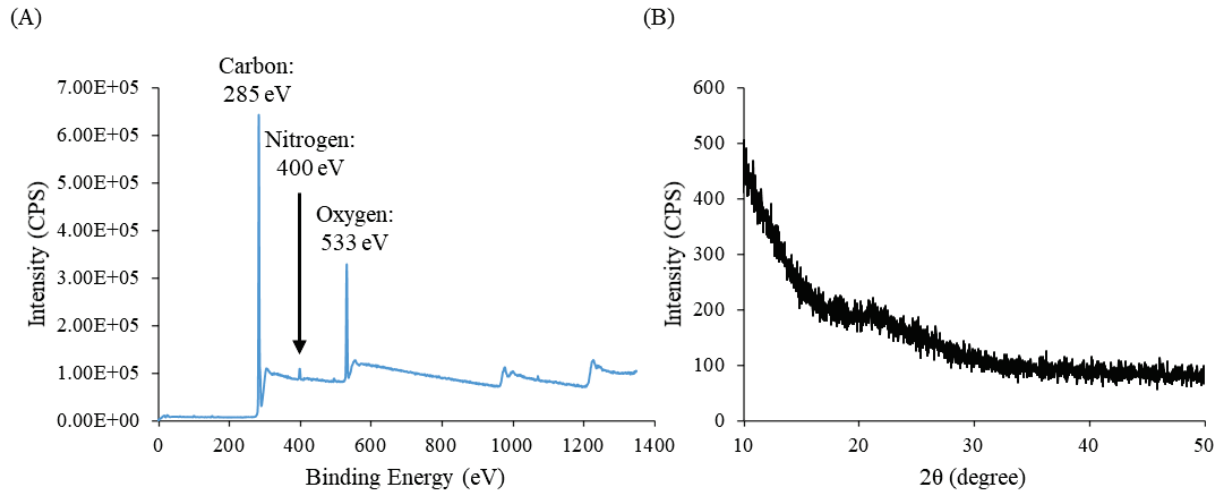

Figure 5: (A) XPS spectrum of the vacuum dried PGQDs shows carbon, nitrogen, and oxygen peaks. (B) XRD spectrum of dried powder PGQDs shows graphene lattice at 20°.

3.3. Optical properties of PGQDs

With the aim of this work being targeted for fluorescence imaging via cell labeling, it is important to acquire information on the PGQDs optical properties. This includes absorption and fluorescence as well as solution condition factors such as pH, concentration, and excitation. The absorption spectrum of PGQDs after synthesis and drying (Figure 6A) showed a decrease in Q-bands from residual TCPP. Furthermore, drying the PGQDs to remove residual TCPP did not impact the fluorescence spectrum which showed a peak excitation of 420 nm that yielded an emission peak at 650 nm (Figure 6B); again, slightly shifted from previously noted TCPP fluorescence of 416 nm excitation and 640 nm emission. This strongly indicates that the red-emission is coming from the PGQDs and not residual TCPP in solution. Additionally, changing the excitation light for the PGQDs (Figure 6C) shows no radiation dependent behavior as there is no noted red-shifting with increasing excitation light was seen with GQDs previously. The PGQDs do, however, show concentration dependency (Figure 6D) as increasing concentrations of PGQDs increases the fluorescence intensity. This is vital due to porphyrins known self-quenching tendencies[33,34] with increasing

concentration due to association and thus the attachment of TCPP to the GQDs has aided in removing this self-quenching characteristic.

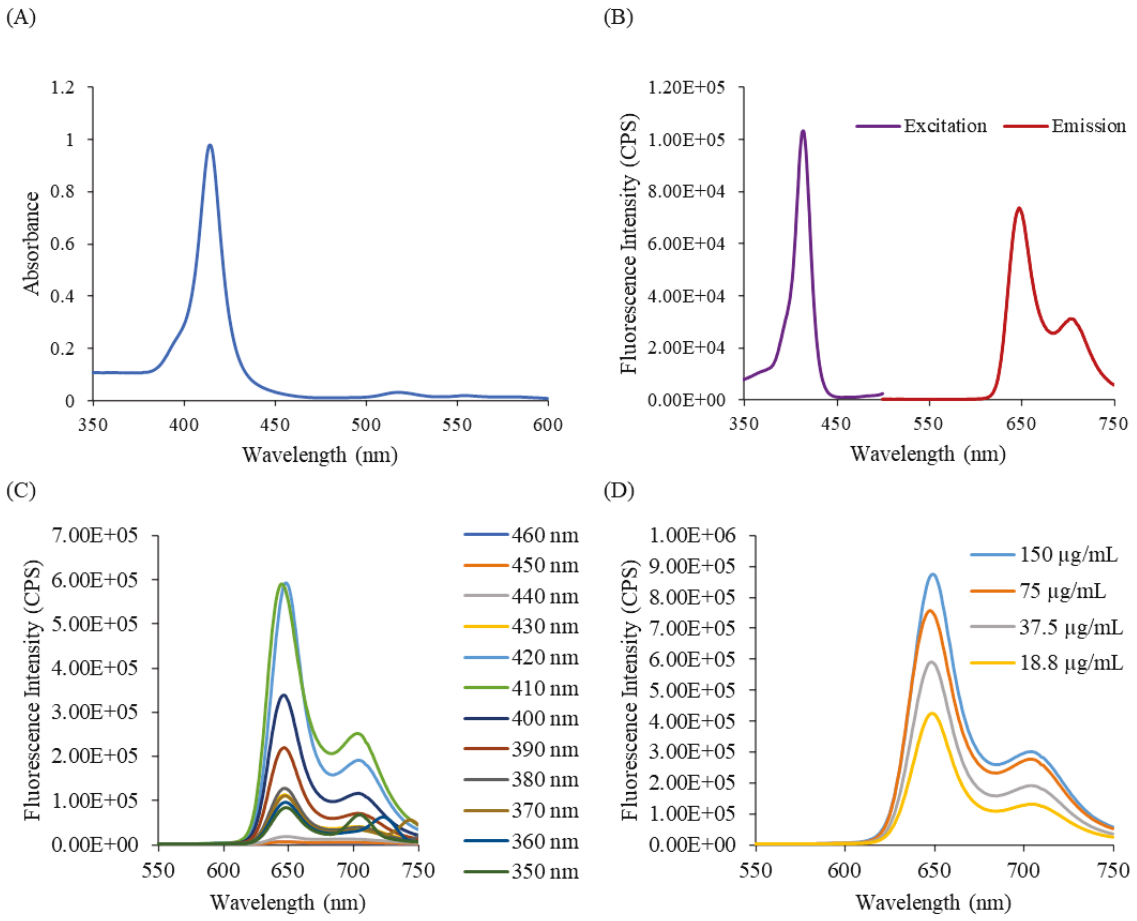

Figure 6: Optical properties of PGQDs. (A) Absorption profile of PGQDs. (B) Excitation (420 nm) and emission (650 nm) fluorescence spectrum of PGQDs (37.5 µg/mL) in 20 mM HEPES pH 7.0 buffer. (C) Changing excitation light for PGQDs depicts excitation-dependent properties. (D) Changing concentration of PGQDs.

Additionally, for the use of these PGQDs in bioanalysis and bioimaging, the stability and potential quenching of these particles in different pHs is critical to determine. Negatively surface charged GQDs are well known to experience quenching in acidic conditions, such as pH 1.0, due to full protonation of oxygen and carboxy functional groups[35,36] leading to agglomeration. Therefore, the PGQDs fluorescence were tested in the same pH range of 1.0 - 11.0 where the fluorescence decreases linearly until pH 6.5, where it drastically drops to near zero fluorescence intensity at pH 5.0, 3.0, and 1.0. Fluorescence quenching at pH 3.0 - 5.0 is attributed to the agglomeration of carbon-based particles in acidic conditions and the degradation of the π-bonds in the porphyrin ring[37] of the PGQDs rather

than agglomeration due to the zeta potential analysis previously discussed (section 3.2.1) showing particle stability and little to no agglomeration of the PGQDs in pH 1.0 - 5.0 (Figure 7).

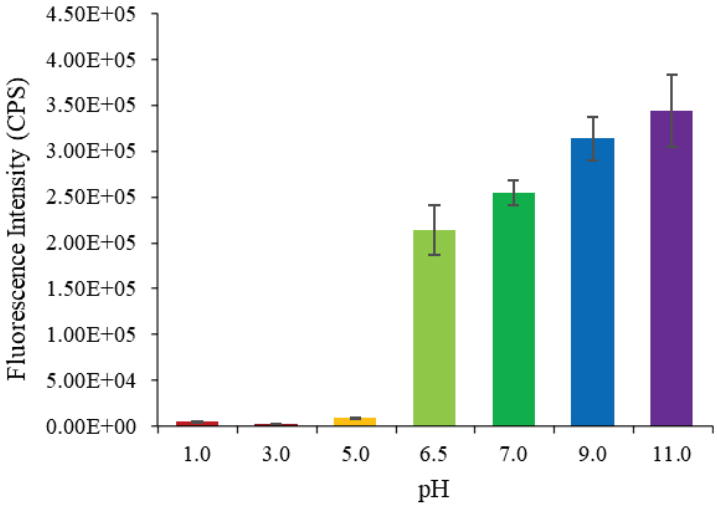

Figure 7: Fluorescence intensity measurements of the PGQDs shows quenching effects in maelate pH 1.0 and citrate pH 3.0 – 5.0 while neutral and basic pHs of 6.5 – 11.0 (HEPES 6.5 – 7.0, CHES 9.0, and CAPS 11.0) depict an increasing fluorescence signal with the more alkaline the solution becomes. All solutions were 190 µg/mL PGQDs.

However, the stability and maintenance of fluorescence in the neutral pHs is encouraging for the biological application of cell imaging these PGQDs are targeted for. However, TCPP and other porphyrins are well known for their poor photostability[38,39] and therefore vital for the application of cell labeling to improve the photostability for prolonged analyses and cell imaging without the fluorescence signal being lost. Therefore, the photostability of the PGQDs was examined in comparison to previously made GQDs from CBDA-2[24] and FITC dye as a standard (Figure 8). After 30 min of excitation light exposure, the PGQDs (excitation 420 nm, emission 650 nm) decreased to 63.7% of their original intensity compared to 67.1% of the GQDs (excitation 310 nm, emission 440 nm). FITC (excitation 495 nm, emission 519 nm) decreased to 8.7% after the 30 min trial, losing 80% of its original intensity in the first 700 sec. Therefore, it can be concluded that the PGQDs exhibit exceptional photostability for prolonged analysis applications.

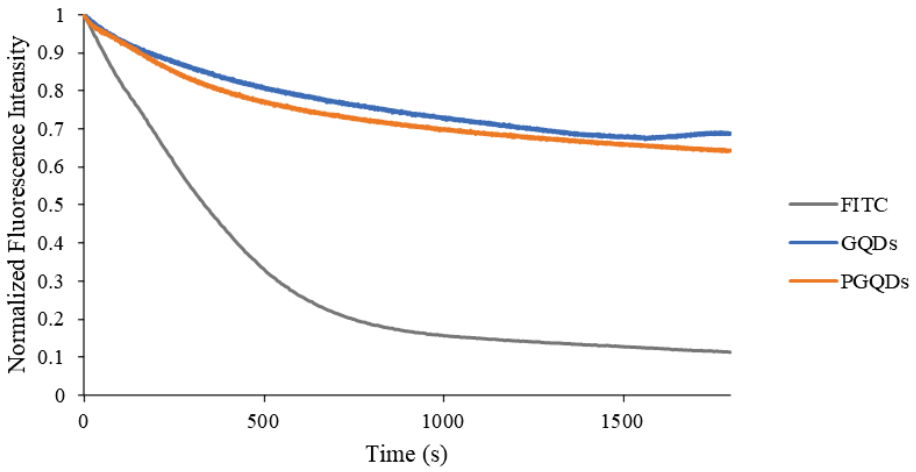

Figure 8: Photostability of FITC, GQDs, and PGQDs. FITC was prepared in 20 mM CHES pH 9.0 while both GQDs and PGQDs were in 20 mM HEPES pH 7.0.

3.4. In vitro *cell imaging and metal ion interference analysis*

The feasibility of the particles to be used as fluorescent agents in cell staining was examined as well to determine particle-cell compatibility. For this purpose, the cytotoxicity was evaluated, utilizing the LDH assay with HeLa cells for 24 h incubation. The results (Figure 9) show negligible toxicity in comparison to the control group with PGQDs up to 200 µg/mL, strongly indicating superior biocompatibility of the PGQDs, although there is some evidence of graphene-based particle toxicity at concentrations higher than 500 µg/mL[40,41].

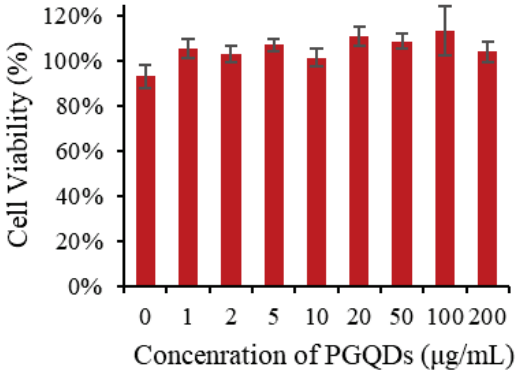

Figure 9: LDH assay results of PGQDs incubated with HeLa cells 24 h at various concentrations.

The negligible cytotoxicity results indicated that the PGQDs might be used as fluorescent cell staining agents. To test this idea, HeLa cells were incubated with PGQDs for 3 h before the cells were fixed and imaged via

fluorescence confocal microscopy using the Alexa 488 channel. Control HeLa cells with no PGQDs were imaged (Figure 10A) along with the brightfield image of the cells demonstrating minimal basal autofluorescence (Figure 10B). However, the HeLa cells with PGQDs (Figure 10C) demonstrated robust staining verifying cellular uptake of the PGQDs. Brightfield imaging verified an intact morphologic phenotype of the PGQDs treated cells consistent with no toxicity at this concentration (Figure 10D).

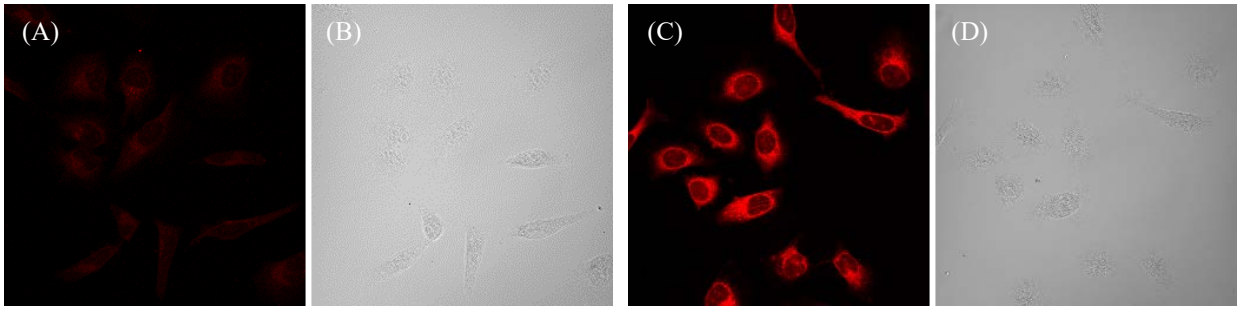

Figure 10: (A) HeLa cells with no PGQDs. (B) Brightfield of blank HeLa cells. (C) 20 µg PGQDs incubated with HeLa cells. (D) Brightfield of PGQDs with HeLa cells.

Lastly, with porphyrins being known to be sensitive to metal ions[42-46], various metal ions were tested to ensure that the natural concentration of metals in biological systems would not interfere with the fluorescence intensity of the PGQDs. Metal ions of Fe^{3+}, Fe^{2+}, Cu^{2+}, Pb^{2+}, and Hg^{2+} were analyzed at concentrations of 1, 5, 10, and 50 µM (Figure 11). Fe^{3+} and Fe^{2+} showed the least quenching up to 50 µM. Pb^{2+} showed the most linear decrease in fluorescence intensity with increasing concentrations. Cu^{2+} showed the greatest quenching, dropping to less than 50% of the original fluorescence intensity at 5.0 µM, and was completely quenched at 50 µM. Hg^{2+} only slightly decreased up to 10 µM but then quenched to 40% fluorescence intensity with 50 µM. However, with no significant quenching with the lowest concentration of metal ions (1.0 µM), it is safe to confirm that the natural concentrations of metal ions in biological systems would not significantly impact the fluorescence intensity of the PGQDs negatively.

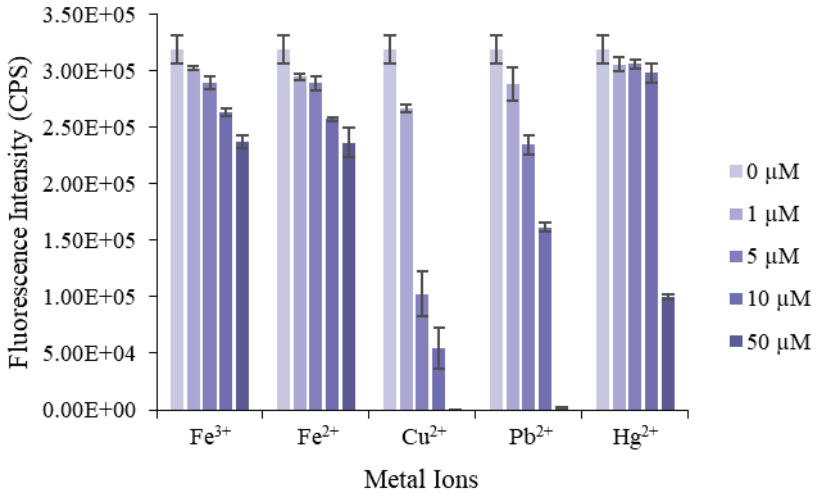

Figure 11: Metal ion analysis at various concentrations with 20 µg/mL PGQDs in 20 mM HEPES buffer pH 7.0.

4. Conclusions

Slight modification to the GQDs synthesis by using ethylenediamine instead of NH_4OH and introducing TCPP yielded red-emissive particles with similar quantum yield (46.6%). After drying the PGQDs at 60 °C, residual TCPP was successfully removed from the material. TEM and HRTEM images showed particles of 7.51 nm with an internal graphene lattice and some larger particle clusters, which resulted in the PGQDs being sonicated to help alleviate the agglomeration. DLS showed that the PGQDs agglomeration was proportional to concentration and sonication time. Lower concentrations of PGQDs required less sonication time, otherwise agglomeration would spike. Similarly, higher concentrations of PGQDs required longer sonication times yet had a time cut-off before agglomeration would worsen drastically. XPS, XRD, and FT-IR confirmed the presence of carbon-nitrogen bonds in the PGQDs as well as a graphene lattice. Zeta potential also indicated the presence of nitrogen as the particles were stable in acidic and basic pHs. However, fluorescence quenching was observed for pHs > 6.5, most likely due to degradation of TCPP π-bonds in the porphyrin ring.

The various fluorescence spectra of the PGQDs shows a slightly shifted excitation and emission peak compared to TCPP, as well as a concentration dependency. However, no radiation dependency was noted, which was present in the GQDs also synthesized from CBDA-2. Cytotoxicity results showed negligible difference between the various concentration of PGQDs compared to the blank control, up to 200 µg/mL. *In vitro* confocal microscopy images

of PGQDs incubated with HeLa cells showed exceptional particle integration into the cells that resulted in clear images for cell staining applications.

Acknowledgements

This work was supported by the NSF grant CHE 1709160 and NSF EPSCoR RII Track I Cooperative Agreement 1946202. Imaging studies were conducted in the UND Imaging Core facility supported by NIH grant P20GM113123, DaCCoTA CTR NIH grant U54GM128729, and UNDSMHS funds. We would also like to formally thank Henrietta Lacks and her family for the contribution of HeLa cells.

Author Information

Corresponding Author:

Julia Zhao – University of North Dakota, Department of Chemistry, 151 Cornell St. Grand Forks, ND 58202, USA; Email: julia.zhao@und.edu

Authors:

Sarah Reagen – University of North Dakota, Department of Chemistry, 151 Cornell St. Grand Forks, ND 58202, USA; Email: sarah.reagen@und.edu

Yingfen Wu – University of North Dakota, Department of Chemistry, 151 Cornell St. Grand Forks, ND 58202, USA 58202; Email: yingfen.wu@und.edu

Rahul Shahni – University of North Dakota, Department of Chemistry, 151 Cornell St. Grand Forks, ND 58202, USA 58202; Email: rahul.shahni@und.edu

Wen Sun – University of North Dakota, Department of Chemistry, 151 Cornell St. Grand Forks, ND 58202, USA 58202; Email: wen.sun@und.edu

Jin Zhang – University of North Dakota, Institute for Energy Studies, 151 Cornell St. Grand Forks, ND 58202, USA 58202; Email: jin.zhang.1@und.edu

Qianli Chu – University of North Dakota, Department of Chemistry, 151 Cornell St. Grand Forks, ND 58202, USA 58202; Email: qianli.chu@und.edu

Xiaodong Hou – University of North Dakota, Institute for Energy Studies, 151 Cornell St. Grand Forks, ND 58202, USA 58202; Email: xiaodong.hou@und.edu

Colin Combs – University of North Dakota, Department of Biomedical Sciences, 151 Cornell St. Grand Forks, ND 58202, USA 58202; Email: colin.combs@und.edu

References

1. Chen, W.; Lv, G.; Hu, W.; Li, D.; Chen, S.; and Dai, Z. Synthesis and applications of graphene quantum dots: a review. *Nanotechnol Rev.* **2018**, *7(2)*, 157-185.
2. Tadyszak, K.; Wychowaniec, J.; and Litowczenko, J. Biomedical applications of graphene-based structures. *Nanomaterials.* **2018**, *8*, 944-964.
3. Jovanović, S.; Syrgiannis, Z.; Marković, Z.; Bonasera, A.; Kepić, D.; Budimir, M.; Milivojević, D.; Spasojević, V.; Dramićanin, M.; Pavlović, V.; and Todorović Marković, B. Modification of structural and luminescence properties of graphene quantum dots by gamma irradiation and their application in a photodynamic therapy. *ACS Appl. Mater. Interfaces.* **2015**, *7*, 25865-25874.
4. Mansuriya, B.; and Altintas, Z. Applications of graphene quantum dots in biomedical sensors. *Sensors.* **2020**, *20(4)*, 1072.
5. Wang, B.; Shen, J.; Huang, Y.; Liu, Z.; and Zhuang, H. Graphene quantum dots and enzyme-coupled biosensors for highly sensitive determination of hydrogen peroxide and glucose. *Int. J. Mol. Sci.* **2018**, *19(6)*, 1696.
6. Ayilliath, S.; Nair, S.; Lakshmi, G.; and Kunnatheery, S. Functionalized graphene quantum dots for cholesterol detection in human blood serum. *J. Fluoresc.* **2021**, *31(3)*, 847-852.
7. Raj. S.; Yadav, V.; Bhadu, G.; Patidar, R.; Kumar, M.; and Kulshrestha, V. Synthesis of highly fluorescent and water soluble graphene quantum dots for detection of heavy metal ions in aqueous media. *Envir. Sci. Pollut. Res. Int.* **2021**, *28(34)*, 46336-46342.
8. Shah, H.; Xie, W.; Wang, Y.; Jia, X.; Nawaz, A.; Xin, Q.; Song, M.; and Gong, J. Preparation of blue- and green-emissive nitrogen-doped graphene quantum dots from graphite and their application in bioimaging. *Mater. Sci. Eng. C.* **2021**, *119*, 111643.

9. Minati, L.; and Del Piano, A. Facile synthesis of water-soluble, highly-fluorescent graphene quantum dots from graphene oxide reduction for efficient cell labelling. *C.* **2019**, *5(4)*, 77.
10. Polesskaya, O.; Baranova, A.; Bui, S.; Kondratev, N.; Kananykhina, E.; Nazarenko, O.; Shapiro, T.; Nardia, F.; Kornienko, V.; Chandhoke, V.; Stadler, I.; Lanzafame, R.; and Myakishev-Rampel, M. Optogenetic regulation of transcription. *Neurosci.* **2018**, *19*, 12-23.
11. Liu, K.; Song, S.; Sui, L.; Wu, S.; Jing, P.; Wang, R.; Li, Q.; Wu, G.; Zhang, Z.; Yuan, K.; and Shan, C. Efficient red/near-infrared-emissive carbon nanodots with multiphoton excited upconversion fluorescence. *Adv. Sci.* **2019**, *6*, 1900766.
12. Pan, L.; Sun, S.; Zhang, A.; Jiang, K.; Zhang, L.; Dong, C.; Huang, Q.; Wu, A.; and Lin, H. Truly fluorescent excitation-dependent carbon dots and their applications in multicolor cellular imaging and multidimensional sensing. *Adv. Mater.* **2015**, *27*, 7782-7787.
13. Kuo, W.; Shen, X.; Chang, C.; Kao, H.; Lin, S.; Wang, J.; and Wu, P. Multiplexed graphene quantum dots with excitation-wavelength-independent photoluminescence, as two-photon probes, and in ultraviolet-near infrared bioimaging. *ACS Nano.* **2020***, 14*, 11502-11509.
14. Song, Z.; Dai, X.; Li, M.; Teng, H.; Song, Z.; Xie, D.; and Luo, X. Biodegradable nanoprobe based on MnO_2 nanoflowers and graphene quantum dots for near infrared fluorescence imaging of glutathione in living cells. *Microchimica Acta.* **2018**, *185*, 485-493.
15. Campbell, E.; Hasan, M.; Rodriguez, R.; Akkaraju, G.; and Naumov, A. Doped graphene quantum dots for intracellular multicolor imaging and cancer detection. *ACS Biomater. Sci. Eng.* **2019**, *5*, 4671-4682.
16. Yang, D.; Yao, X.; Dong, J.; Wang, N.; Du, Y.; Sun, S.; Gao, L.; Zhong, Y.; Qian, C.; and Hong, H. Design and investigation of core/shell GQDs/hMSN nanoparticles for enhanced drug delivery platform in triple-negative breast cancer. *Bioconjugate Chem.* **2018**, *29*, 2776-2785.
17. Tahoun, M.; Gee, C.; McCoy, V.; Sander, P.; and Müller, C. Chemistry of porphyrins in fossil plants and animals. *RSC Adv*. **2021**, *11*, 7552.
18. Qi, Z.; Cheng, Y.; Xu, Z.; and Chen, M. Recent advances in porphyrin-based materials for metal ions detection. *Int. J. Mol. Sci.* **2020**, *21*, 5839.
19. Ussia, M.; Bruno, E.; Spina, E.; Vitalini, D.; Pellegrino, G.; Ruffino, F.; Privitera, V.; and Carroccio, S. Freestanding photocatalytic materials based on 3D graphene and polyporphyrins. *Sci Rep.* **2018**, *8*, 5001.

20. Hadmojo, W.; Yim, D.; Aqoma, H.; Ryu, D.; Shin, T.; Kim, H.; Hwang, E.; Jang, W.; Jung, I.; and Jang, S. Artificial light-harvesting n-type porphyrin for panchromatic organic photovoltaic devices. *Chem. Sci*. **2017**, *8*, 5095.
21. Jin, G.; He, R.; Liu, Q.; Lin, M.; Dong, Y.; Li, K.; Tang, B.; Liu, B.; and Xu, F. Near-infrared light-regulated theranostic nanoplatform based on aggregation-induced emission luminogen encapsulated upconversion nanoparticles. *Theranostics.* **2019**, *9*, 246-264.
22. Mahajan, P.; Dige, N.; Vanjare, B.; Phull, A.; Kim, S.; Hong, S.; and Lee, K. Synthesis, photophysical properties and application of new porphyrin derivatives for use in photodynamic therapy and cell imaging. *J. Fluoresc.* **2018,** *28*, 871-882.
23. Wang, D.; Zhang, Z.; Lin, L.; Liu, F.; Wang, Y.; Guo, Z.; Li, Y.; Tian, H.; and Chen, X. Porphyrin-based covalent organic framework nanoparticles for photoacoustic imaging-guided photodynamic and photothermal combination cancer therapy. *Biomater.* **2019**, *223*, 119459.
24. Reagen, S.; Wu, Y.; Liu, X.; Shahni, R.; Bogenschuetz, J.; Wu, X.; Chu, Q.; Oncel, N.; Zhang, J.; Hou, X.; Combs, C.; Vasquez, A.; and Zhao, J.X. *ACS Appl. Mater. Inter.* **2021**, *13*, 43952.
25. Li, B.; Wang, X.; Chen, L.; Zhou, Y.; Dang, W.; Chang, J.; and Wu, C. Ultrathin Cu-TCPP MOF nanosheets: a new theragnostic nanoplatform with magnetic resonance/near-infrared thermal imaging for synergistic phototherapy of cancers. *Theranostics.* **2018**, *8(15)*, 4086-4096.
26. Jia, Y.; Li, F.; Jia, T.; and Wang, Z. Meso-tetra(4-carboxylphenyl)porphine-enhanced DNA methylation sensing interface on a light-addressable potentiometric sensor. *ACS Omega*. **2019**, *4*, 12567-12574.
27. Wang, Z.; Elliot, Q.; Wang, Z.; Setien, R.; Puttkammer, J.; Ugrinov, A.; Lee, J.; Webster, D.; and Chu, Q.R. Fufural-derived diacid prepared by photoreaction for sustainable materials synthesis. *ACS Sustain. Chem. Eng.* **2018**, *6*, 8136-8141.
28. Horiba, https://www.horiba.com/en_en/applications/materials/material-research/quantum-dots/recording-fluorescence-quantum-yields/, accessed 24 November 2021.
29. Wu, J.; Wang, W.; and Wang, Z. Porphin-based carbon dots for "turn off-on" phosphate sensing and cell imaging. *Nanomater.* **2020**, *10*, 326.

30. Zhang, X.; Hou, L.; Richard, F.; and Samorì, P. Modular preparation of graphene-based functional architectures through two-step organic reactions: towards high-performance energy storage. *Chemistry*. **2018**, *24(69)*, 18518.

31. Liu, Q.; Li, H.; Zhao, Q.; Zhu, R.; Yang, Y.; Jia, Q.; Bian, B.; and Zhuo, L. Glucose-sensitive colorimetric sensor based on peroxidase mimics activity of porphyrin-Fe_3O_4 nanocomposites. *Mater. Sci. Eng. C.* **2014**, *41*, 142-151.

32. Nair, R.; Thomas, R.; Sankar, V.; Muhammad, H.; Dong, M.; and Pillai, S. Rapid, Acid-free Synthesis of High-quality Graphene Quantum Dots for Aggregation Induced Sensing of Metal Ions and Bioimaging. *ACS Omega.* **2017**, *2*, 8051-8061.

33. Shaikh, S.; Chakraborty, A.; Alatis, J.; Cai, M.; Danilov, E.; and Morris, A. Light harvesting and energy transfer in a porphyrin-based metal organic framework. *Faraday Discuss.* **2019**, *216*, 174-190.

34. Dehaen, R.; Vaz Serra, V.; Botequim, D.; Paulo, P.; Andrade, S.; and Costa, S. Fluorescence spectroscopy of porphyrins and phthalocyanines: some insights into supramolecular self-assembly, microencapsulation, and imaging microscopy. *Molecules.* **2021**, *26(14)*, 4264.

35. Yoon, H.; Park, M.; Kim, J.; Novak, T.; Lee, S.; and Jeon, S. Toward highly efficient luminescence in graphene quantum dots for optoelectronic applications. *Chem. Phys. Rev.* **2021**, *2(3)*, 031303.

36. Liu, C.; Zhang, F.; Hu, J.; Gao, W.; and Zhang, M. A mini review on pH-sensitive photoluminescence in carbon nanodots. *Front. Chem.* **2021**, *8*, 605028.

37. Choi, M.; Pollard, J.; Webb, M.; and McHale. J. Counterion-dependent excitonic spectra of tetra(p-carboxyphenyl)porphyrin aggregates in acidic aqueous solution. *J. Am. Chem. Soc.* **2003**, *125(3)*, 810-820.

38. Hassan, G.; El Hoda Saad, N.; Hmadeh, M.; and Karam, P. Enhancing porphyrin photostability when locked in metal-organic frameworks. *Dalton Trans.* **2018**, *47*, 15765-15771.

39. Sulek, A.; Pucelik, B.; Kobielusz, M.; Barzowska, A.; and Dabrowski, J. Photodynamic inactivation of bacteria with porphyrin derivatives: effect of charge, lipophilicity, ROS generation, and cellular uptake on their biological activity in vitro. *Int. J. Mol. Sci.* **2020**, *21*, 8716.

40. Fasbender, S.; Allani, S.; Wimmenauer, C.; Cadeddu, R.; Raba, K.; Fischer, J.; Bulat, B.; Luysberg, M.; Seidel, C.; Heinzel, T.; and Haas, R. Uptake dynamics of graphene quantum dots into primary human blood cells following in vitro exposure. *RSC Adv.* **2017**, *7*, 12208-12216.

41. Perini, G.; Palmieri, V.; Ciasca, G.; De Spirito, M.; and Papi, M. Unravelling the potential of graphene quantum dots in biomedicine and neuroscience. *Int. J. Mol. Sci.* **2020**, *21*, 3712.

42. Wei, K.; Yao, F.; and Kang, X. Single-molecule porphyrin-metal ion interaction and sensing application. *Biosens. Bioelectron.* **2018**, *109*, 272-278.

43. Wang, Q.; Ke, W.; Lou, H.; Han, Y.; and Wan, J. A novel fluorescent metal-organic framework based on porphyrin and AIE for ultra-high sensitivity and selectivity detection of Pb^{2+} ions in aqueous solution. *Dyes Pigm.* **2021**, *196*, 109802.

44. Ermakova, E.; Koroleva. E.; Shokurov, A.; Arslanov, V.; and Kessmertnykh-Lemeune, A. Ultra-thin film sensors based on porphyrin-5-ylphosphonate diesters for selective and sensitive dual-channel optical detection of mercury (II) ions. *Dyes Pigm.* **2021**, *186*, 108967.

45. Fu, C.; Sun, X.; Zhang, G.; Shi, P.; and Chu, P. Porphyrin-based metal-organic framework probe: highly selective and sensitive fluorescent turn-on sensor for M^{3+} (Al^{3+}, Cr^{3+}, and Fe^{3+}) ions. *Inorg. Chem.* **2021**, *60*, 1116-1123.

46. Qi, Z.; Cheng, Y.; Xu, Z.; and Chen, M. Recent advances in porphyrin-based materials for metal ion detection. *Int. J. Mol. Sci.* **2020**, *21*, 5839.

For Table of Contents Use Only